Rare Met. (2015) 34(10):683–691
DOI 10.1007/s12598-015-0475-8

RARE METALS
www.editorialmanager.com/rmet

Microwave-assisted synthesis of L-cysteine-capped nickel nanoparticles for catalytic reduction of 4-nitrophenol

Nazar Hussain Kalwar, Ayman Nafady, Razium Ali Soomro*, Sirajuddin, Syed Tufail Hussain Sherazi, Abdul Rauf Khaskheli, Keith Richard Hallam

Received: 17 September 2014 / Revised: 31 January 2015 / Accepted: 12 March 2015 / Published online: 24 May 2015

Abstract A simple and efficient microwave-assisted procedure for synthesis of L-cysteine-capped nickel nanoparticles (cyst-Ni NPs) in ethylene glycol solvent was demonstrated. The as-synthesised NPs were characterised by ultraviolet–visible (UV–Vis) spectrophotometer, Fourier transform infrared (FTIR) spectroscopy, transmission electron microscopy (TEM) and X-ray diffractometry (XRD). The cyst-Ni NPs are proved to be excellent heterogeneous catalysts for the 100 % reduction of 4-nitrophenol (4-NPh) in the presence of reductant ($NaBH_4$) within reaction time of 40 s. In contrast, Raney nickel in similar sample environments shows only 25.5 % reduction. The kinetic and energetic behaviours of cyst-Ni NPs were also studied, and the reduction reaction is determined to follow pseudo-first-order kinetics with a rate constant value of 0.115 s^{-1} and activation energy of 36.1 $kJ \cdot mol^{-1}$. In addition to its high catalytic competence, cyst-Ni NPs catalyst exhibits excellent recyclability with negligible catalytic poisoning.

Keywords L-cysteine; Nickel nanoparticles; Catalyst; Reduction of 4-nitrophenol

1 Introduction

Nickel nanoparticles (Ni NPs) are considered special due to their magnetic properties and high catalytic potential compared with ordinary nickel plate. They are the most promising candidates to substitute for platinum conducting electrolytic membranes in fuel cells, which could reduce the cost of internal combustion engine operation [1]. Several methods, such as radiation [2], micro-emulsion [3], thermal decomposition [4, 5], laser ablation [6, 7] and aqueous chemical reduction [8], are used for preparation of Ni NPs. However, the aqueous reduction route is preferred for its simplicity, inexpensiveness and ease of control over particle size and distribution via common experimental parameters [9–12]. Hou et al. [13] reported the synthesis of stable Ni NPs using wet chemical methodology with hexadecylamine (HDA) and trioctylphosphine oxide (TOPO) as protecting agents. Similarly, Roselina et al. [14] demonstrated the formation of nickel nanostructures via chemical reduction employing hydrazine and ethylene glycol as the reducing and stabilising agents, respectively. And very recently, Tontini et al. [15] reported the synthesis of temperature-controlled loose nickel micro-urchins using a chemical reduction route. From the present literature perspective, it is clear that the development of a feasible synthetic method for NPs is important to support their use in various practical applications. This applies particularly to Ni NPs that are very much vulnerable towards oxidation

N. H. Kalwar, R. A. Soomro*, Sirajuddin, S. T. H. Sherazi, A. R. Khaskheli
National Centre of Excellence in Analytical Chemistry, University of Sindh, Jamshoro 76080, Pakistan
e-mail: raziumsoomro@gmail.com

A. Nafady
Department of Chemistry, College of Science, King Saud University, Riyadh 11451, Saudi Arabia

R. A. Soomro, K. R. Hallam
Interface Analysis Centre, School of Physics, University of Bristol, Bristol BS8 1TL, UK

A. R. Khaskheli
Department of Pharmacy, Shaheed Mohtarma Benazir Bhutto Medical University, Larkana 77150, Pakistan

[16]. The extent of this surface oxidation increases with the decrease in average particle diameter, which as a consequence is responsible for diminished catalytic performance [17]. Tremendous efforts were carried out for the preparation of pure metallic nanosized Ni NPs through various synthesis strategies. Ajeet et al. [18] reported the controlled synthesis of Ni NPs using water and oil microemulsions. In contrast, Wu and Chen [19] reported the formation of spherical Ni NPs by the hydrazine reduction of nickel chloride in ethylene glycol solvent, and recently, Roy and Bhattacharya [20] addressed the use of polymers to produce air–durable Ni NPs. However, all such strategies either include the application of inert atmosphere, toxic reducing agents or dense molecular weight polymers as capping/protecting agents for stability; this, as a consequence, restricts the large volume production and application of Ni NPs in various catalytic reactions.

In connection to the application of metal NPs in various fields, the use of nanosized metal structures as heterogeneous recyclable catalysts in environmental applications is needed now. In particular, nitrophenols (NPhs) are considered among the ingredients that contaminate the aquatic environment via their discharge from numerous industries. The extreme nature of such toxic materials is reflected in the 10 $ng{\cdot}L^{-1}$ permissible limit prescribed by the US Environmental Protection Agency for 2,4-dinitrophenol, 2-NPh and 4-NPh in natural waters [21]. Presently used treatment and detoxification methods for such toxic materials include adsorption, biological, coagulation routes and ozonation [22]. However, such processes suffer from cons such as time consumption, expensive procedures, inefficient treatment and secondary pollution, causing increases in overall cost because of extra disposal procedures. It is known that Ni NPs are used for the synthesis of 4-aminophenol (4-APh) from 4-NPh [23]. Thus, the application of nanosized nickel for reduction of 4-NPh would allow both the formation of 4-APh and detoxification of 4-NPh, reducing the overall input of carcinogenic compounds in aquatic environment.

It was mainly due to such consideration that the present study was targeted towards microwave-assisted fabrication of pure metallic Ni NPs via aqueous reduction employing L-cysteine as an effective capping agent and Na_2CO_3 as a mild reducing agent. The as-synthesised Ni NPs were known to exhibit enhanced catalytic reduction capability compared to that of Reney nickel used for the reduction of 4-NPh. In addition, this study also highlights the catalytic kinetic and energetic behaviour of L-cysteine-capped nickel nanoparticles (cyst-Ni NPs) during reduction, based on which we believe the best route for the formation of aminophenol from nitrophenol was presented here.

2 Experimental

2.1 Materials

Analytical grade nickel (II) chloride hexahydrate ($NiCl_2{\cdot}6H_2O$), sodium borohydride ($NaBH_4$), sodium carbonate (Na_2CO_3), acetone ($(CH_3)_2CO$) and methanol (CH_3OH) were purchased from E. Merck, while L–cysteine ($C_3H_7NO_2S$), ethylene glycol ($C_2H_6O_2$) and sodium hydroxide (NaOH) were purchased from Fluka Chemicals. 4-nitrophenol ($C_6H_5NO_3$; 4-NPh) was purchased from Fisher Scientific Laboratory Suppliers (FSA). All chemicals and reagents were used as received.

2.2 Synthesis of L-cysteine-capped Ni NPs

Cyst-Ni NPs were synthesised by mixing 0.3 ml of 0.01 $mol{\cdot}L^{-1}$ Na_2CO_3 and 1 ml of 0.01 $mol{\cdot}L^{-1}$ $NiCl_2{\cdot}6H_2O$ in a conical flask followed by addition of 0.1 ml of 0.1 $mol{\cdot}L^{-1}$ NaOH and 0.6 ml of 0.01 $mol{\cdot}L^{-1}$ L-cysteine and dilution to 6.0 ml with ethylene glycol. This mixture was placed in a domestic microwave oven (Glanz 900 W) for 60 s. The colour of solution turned from transparent to brown and then to dark black at intervals of about 10 s. The hot black colloidal dispersion was then removed carefully from inside the microwave oven and cooled quickly in an ice water bath. As soon as the sample reached room temperature, it was transferred to a 1-cm quartz cell to be optically characterised using ultraviolet–visible (UV–Vis, Perkin–Elmer, Lambda 2) spectroscopy.

2.3 Sample preparation and characterisation

A large volume (1000 ml) of a black colloidal solution of cyst-Ni NPs was prepared, transferred to petri dishes (in small volumes) and dried in a water bath at 100 °C. The product was cooled to room temperature and washed several times with methanol and deionised water. The product was then dried in an oven at 110 °C for 30 min. The obtained dried product was further cooled in desiccators and then collected onto a clean glass slide for Fourier transform infrared spectroscopy (FTIR, Nicolet 5700) characterisation.

Samples for transmission electron microscopy (TEM, Jeol JEM 1200 EX MKI) were prepared by putting 10 µl drops of cyst-Ni NPs containing sample on carbon-coated copper grids and drying under nitrogen atmosphere for about 1 h. Samples were then fitted in the TEM sample.

Morphological study was carried out using atomic force microscopy (AFM, Agilent 5500), for which 250 $\mu g{\cdot}ml^{-1}$ nanocolloidal solutions were centrifuged for 2 min and sonicated (KQ 500-DE) for 25 min. About 30 µl aliquots of sample were then deposited on freshly cleaved mica surfaces for analysis.

Phase purity and confirmation of cyst-Ni NPs was carried out using X-ray diffraction (XRD, Bruker D-8. A Metrohm Model 781 Meter). A suitable quantity of Ni NPs was prepared by drying sufficient nanocolloidal solution of cyst-Ni NPs under nitrogen to avoid oxidation. The obtained product was washed thoroughly with deionised water and acetone to remove any impurities and unreacted biomolecules followed by dehydrating the sample in a preheated oven at 100 °C.

2.4 Catalytic performance of cyst-Ni NPs

In a representative reduction experiment, specific amounts of cyst-Ni NPs were deposited on pre-weighed glass cover slips and dried under a nitrogen atmosphere to ensure complete adhesion to the surface. These cover slips were then further used for heterogeneous catalytic reduction of 4-NPh. For an un-catalysed reaction, an aqueous solution of 0.4 ml of 0.1 mmol·L^{-1} 4-NPh diluted to 3 ml was taken in a 4-ml capacity quartz cuvette along with 1 ml of 0.15 mol·L^{-1} $NaBH_4$. The reaction mixture was studied with UV–Vis spectrophotometer at room temperature and atmospheric pressure. Similarly, for a catalysed reaction, a glass cover slip with an appropriate amount of cyst-Ni NPs and Raney nickel would be placed inside the sample container containing 4-NPh and reductant solution. Catalysed reactions were followed by measuring the time-dependent decline in absorbance at characteristic peaks of 4-NPh.

2.5 Recovery and reuse of catalyst

The Ni NPs (supported on glass cover slips) used in the reduction of fresh solutions of 4-NPh were removed from the quartz cell and then washed five times with deionised water and dried. These glass-supported Ni NPs were used in a similar way as in Sect. 2.4 for the reduction of fresh solutions of 4-NPh. Such treatment was repeated four times in order to observe any change in the efficiency of Ni NPs for the given reaction.

3 Results and discussion

3.1 UV–Vis analysis of cyst-Ni NPs

Parameters such as concentrations of nickel chloride, L-cysteine and sodium hydroxide solution, pH and heating time of the reaction mixture were studied and optimised. The most stable and small-sized (blue-shifted) Ni NPs are found to exhibit surface plasmon resonance at 386 nm. UV–Vis spectra representing cyst-Ni NPs in fresh, 1- and 2-week old condition under optimised conditions are shown in Fig. 1.

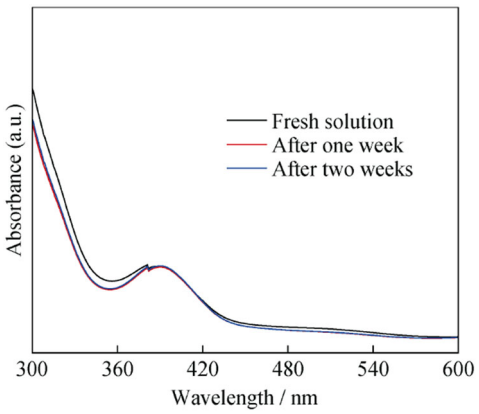

Fig. 1 UV–Vis spectra of L-cysteine-derived Ni NPs

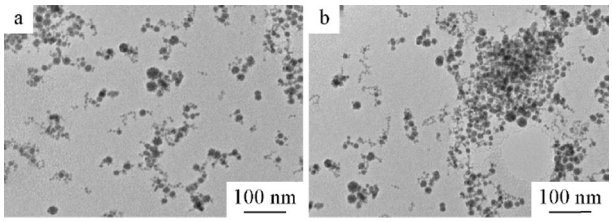

Fig. 2 TEM images recorded for stability of cyst-Ni NPs after **a** 1 and **b** 2 weeks of synthesis

The lack of any change in wavelength and absorbance reveals the high stability of as-synthesised cyst-Ni NPs, which is also evident from the corresponding TEM images presented in Fig. 2. It can be seen that even after 2 weeks of formation, Ni NPs are quite dispersed and maintain their average size at (7.0 ± 2.5) nm. There is no change in solution colour and absorption wavelength even after several more weeks. The broadness in absorption bands is due to the contribution from a few bigger spherical nanoparticles, as mentioned by others [24].

UV–Vis spectra of Ni NPs prepared by taking different Ni^{2+} to L-cysteine molar ratios, such as 1:2, 1:3 and 1:6, show small increases in absorbance and change in maximum absorbance (λ_{max}) from a red-shifted value of 392 nm to a blue-shifted value of 386 nm. This is further confirmed from the TEM images recorded for molar ratios of 1:1 and 1:6, as shown in Fig. 3. It is evident that when Ni^{2+} and L-cysteine were used at 1:1 (Fig. 3a), large populations of formed NPs are non-uniform in size and aggregate with an average size of greater than (25.0 ± 3.5) nm. Such inhomogeneity in particle size and distribution restricts the efficient use of metal NPs for surface-based catalysis, as indicated in several other reports [25–27]. Contrary to this, a molar ratio of 1:6 exhibits uniformity in particle size distribution with an increase in population of formed NPs and an average size of (8.0 ± 1.5) nm, as apparent in Fig. 3b. This clearly suggests that an increase

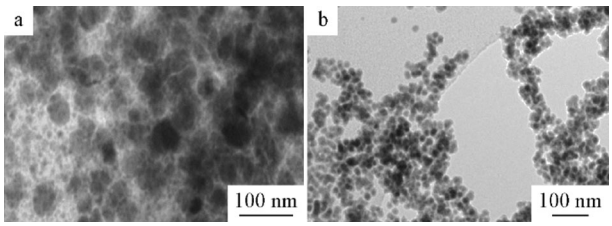

Fig. 3 TEM images recorded for different Ni^{+2} to L-cysteine molar ratio of **a** 1.1 and **b** 1.6

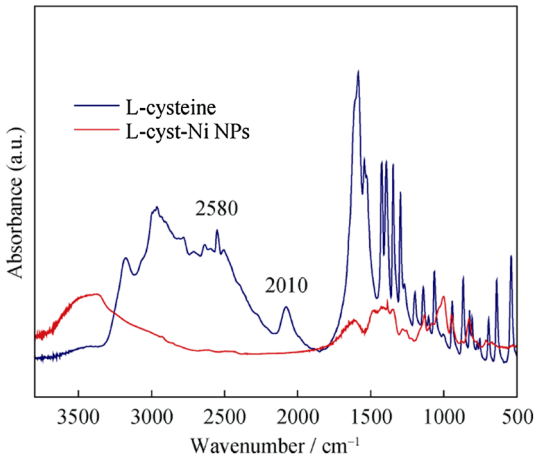

Fig. 4 FTIR spectra of pure L-cysteine and newly synthesised L-cysteine-derived Ni NPs

in concentration of L-cysteine upsurges the formation of metallic Ni NPs along with reduction in size and surface oxidation, as described in Refs. [8, 28].

3.2 FTIR spectra of cyst-Ni NPs

FTIR spectra of L-cysteine and L-cysteine-derived Ni NPs are shown in Fig. 4. The absorption band at 2551 cm^{-1} is characteristic for S–H stretching [29, 30]. This band disappears on coordination of L-cysteine molecules with particle surfaces via thiolate linkages and provides strong evidence for binding of L-cysteine to Ni NPs. This is in good agreement with the results in Ref. [31].

It is clear that the Ni NPs are not linked via either the carboxylate or amino side of L-cysteine because the characteristic bands I and II of the amino acids are present at 1585 and 1544 cm^{-1} in the free L-cysteine but shift to 1608 and 1578 cm^{-1}, respectively (in our case), after the formation of $–CO–NH_2$ [31]. Furthermore, the peak at 2080 cm^{-1} observed in pure L-cysteine for NH^{3+} [32] is absent in the case of cyst-Ni NPs, reflecting the formation of acylamino. The shift towards higher frequency of signals in the range of 2300–3400 cm^{-1} is specific for the collective effect of intra-molecular H-bonding between $–NH_2$ and –OH of L-cysteine, indicative of the formation of new bonding between Ni NPs and L-cysteine thiol groups. Based on these experimental results, a plausible mechanism of formation for cyst-Ni NPs is given in Fig. 5.

At the initial stage, Ni_2CO_3 forms as a result of reaction between Ni^{2+} and Na_2CO_3 in solution. Later, hydrolysis of carbonate results in the release of Ni^{2+} and concurrent reduction to Ni(0). As the concentration of carbonate decreases, there is further dissolution of Ni_2CO_3 to its respective ions, simultaneously reducing all Ni^{2+} to Ni(0) atoms [33]. The formed Ni(0) serves as nuclei for rapid large particle formation, decreasing their surface energy, due to their high interfacial mobility. However, the presence of a large population of L-cysteine molecules restricts particle growth via adsorption onto the formed nuclei. This adsorption leads to a decrease in grain boundary energy which consequently decreases the driving force for particle growth [34, 35]. Contrary to the alkali and $NaBH_4$ reduction method, where fast ion reducing processes hinder the effective protection of NPs [36], the use of a mild reducing agent, such as Na_2CO_3, and the uniform energy transfer from microwave radiation allow the formation of small and uniformly distributed Ni NPs [37]. The use of Na_2CO_3 not only allows slow reduction for uniform nucleation but also gives a short time lag in reduction which, in turn, enhances the effective L-cysteine binding over Ni NPs, leading to high stability and narrow particle size distribution [38].

3.3 TEM observations

Representative TEM images of Ni NPs from the optimised 1:6 molar ratio of Ni to L-cysteine are shown in Fig. 6. These clearly depict that most cyst-Ni NPs particles are small in size. However, some aggregations can be seen due to intra-molecular interactions and peptide bond formation between L-cysteine molecules bound on the surface of Ni NPs. TEM analysis reveals that most particles are spherical in shape with an average size of (7.5 ± 1.5) nm and in the range of 2–32 nm, while abundant particles are 3 nm in size. These small–sized nickel nanospheres present within the biomolecule-assisted agglomerates are responsible for the excellent catalytic activity.

3.4 AFM analysis of cyst-Ni NPs

Surface morphological features of cyst-Ni NPs were observed using tapping mode AFM. Figure 7a shows a vertical scale AFM image of cyst-Ni NPs with spherical and uniform morphological features. The height profiling carried using WSxM software determines that particles have an average height of (14.0 ± 1.8) nm. Figure 7b presents a three-dimensional vertical-grain structure image of NPs

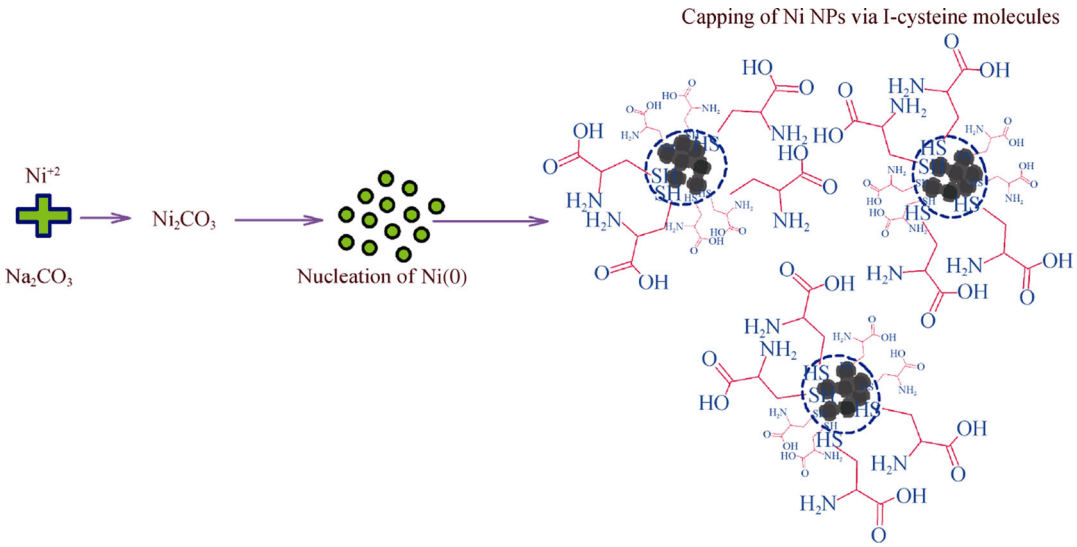

Fig. 5 Capping mechanism for cyst-Ni NPs

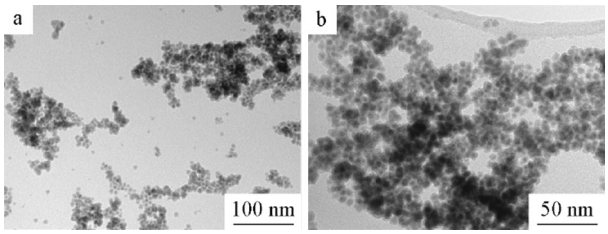

Fig. 6 TEM images of freshly formed L-cysteine-derived Ni NPs by microwave irradiation in ethylene glycol: **a** low resolution, and **b** high resolution

(topographical map), demonstrating the highly rough surface morphology with several dents, ditches and irregularities on the surface of NPs. Such rough surfaces have greater numbers of active sites, providing greater numbers of contact points for catalysis [39, 40].

3.5 XRD pattern of cyst-Ni NPs

In order to reveal the crystal structure of the Ni NPs, XRD analysis was conducted (Fig. 8). The XRD pattern exhibits well-resolved peaks at $2\theta = 44.4°$, 51.6° and 76.8°, indexed to the (111), (200) and (220) planes, respectively, of pure FCC nickel. No characteristic peaks indexed to oxide are observed, indicating the phase purity and confirmation of Ni NPs formation. The pattern obtained is similar to previous report [41].

3.6 Evaluation of catalytic reduction of 4-NPh

The activity of catalyst NPs is usually tested by observing the reduction of aromatic nitro compounds to corresponding amine derivatives in the presence of $NaBH_4$ [42]. Figure 9 presents UV–Vis spectra that demonstrate the reduction of 4-NPh to 4-APh. Figure 9a shows the

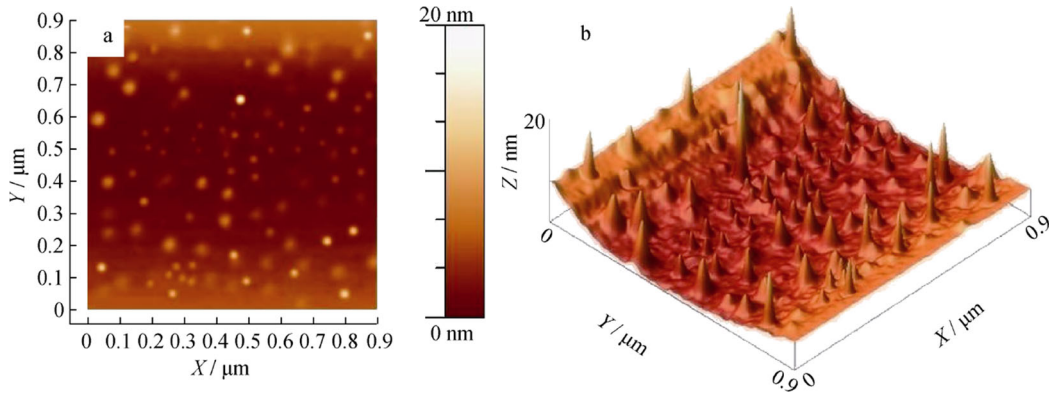

Fig. 7 AFM images of cyst-Ni NPs: **a** typical medium-scale AFM image (0.9 μm × 0.9 μm) of L-cysteine-capped Ni NPs and **b** vertical-grain structure of nickel nanoparticles (topographical map)

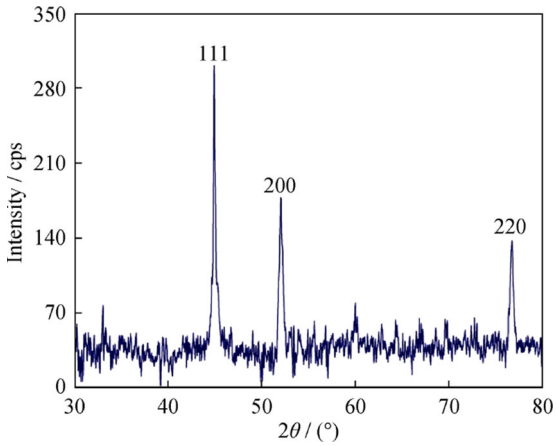

Fig. 8 XRD pattern of cyst-Ni NPs

formation of 4-nitrophenolate ions produced by treating the solution of 4-NPh with $NaBH_4$. 4-NPh is converted to 4-nitrophenolate via the removal of a proton in the presence of $NaBH_4$ and UV light. The peaks at 317 and 400 nm are characteristics of 4-NPh and 4-nitrophenolate ions in aqueous medium and the absence and presence of $NaBH_4$, respectively [32]. The 4-nitrophenolate ions are rapidly converted into 4-APh in the presence of Ni NPs as a result of rapid hydrogen transfer from $NaBH_4$, with the appearance of a corresponding peak at 300 nm. The following schematic equation represents the catalytic reduction of 4-NPh to 4-APh in the presence of catalyst (cyst-Ni NPs), where black circles represent Ni NPs catalyst.

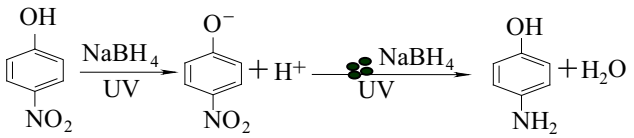

(1)

Figure 9b shows the reduction of 4-nitrophenolate ions to 4-APh using varying amounts (0.1 and 0.2 mg) of Ni NPs in the presence of $NaBH_4$. Each spectrum was recorded at 40 s after catalyst insertion. In contrast, Fig. 9c presents the reduction of 4-NPh by varying amounts (0.1 and 0.2 mg) of Raney nickel (powder) in similar sample environment and after the same reaction time.

Comparison of these spectra clearly shows that the reductions of 4-NPh by 0.1 and 0.2 mg cyst-Ni NPs are 67.5 % and 100.0 %, respectively, while under similar conditions Raney nickel shows only 9.6 % and 25.5 % reduction. These results clearly demonstrate the relative efficiency of two similar catalysts based on size alteration.

3.7 Kinetics and thermodynamics of 4-NPh reduction

The kinetics of heterogeneous catalysis are best determined using the Langmuir–Hinshelwood (L–H) model [30], given as:

$$-\frac{dC}{dt} = \frac{k_{L-H}k_{ad}C}{1 + k_{ad}C} \tag{2}$$

where k_{L-H} is the reduction reaction rate constant, k_{ad} is the adsorption coefficient of 4-NPh on Ni NPs (catalyst) and C describes the variable concentration at any time t. As values of $k_{ad}C$ for pseudo-first-order kinetics are much smaller compared to 1 in the denominator, Eq. (2) can be simplified as:

$$\ln\left(\frac{C_0}{C}\right) = k_{L-H}k_{ad}t = -kt \tag{3}$$

where C_0 represents the initial concentration of 4-NPh and $k = k_{L-H}k_{ad}$ is the pseudo-first-order reaction rate constant.

Figure 10a shows linear regression analysis of a plotted graph of natural logarithm for ratio of initial concentration for 4-NPh and its relative remaining concentration during catalytic reduction against the corresponding reaction time. The reaction rate constant for reduction is determined to be 0.115 s^{-1} with a corresponding coefficient of regression

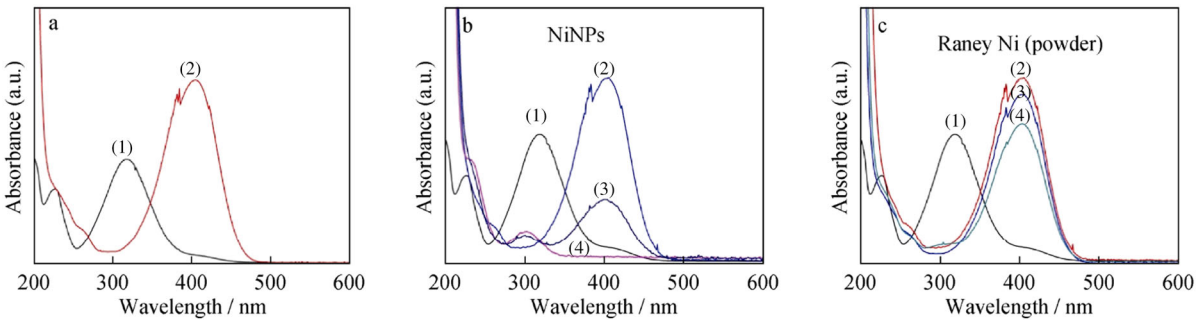

Fig. 9 UV–Vis spectra for: **a** (1) 10 μmol·L^{-1} aqueous solution of 4-NPh, (2) 10 μmol·L^{-1} 4-NPh in the presence of 0.15 mol·L^{-1} $NaBH_4$; **b** as **a** plus reduction of 10 μmol·L^{-1} 4-NPh with (3) 0.1 mg Ni NPs, (4) 0.2 mg Ni NPs; **c** as **a** plus reduction of 10 μmol·L^{-1} 4-NPh with (3) 0.1 mg Raney nickel powder, (4) 0.2 mg Raney nickel powder

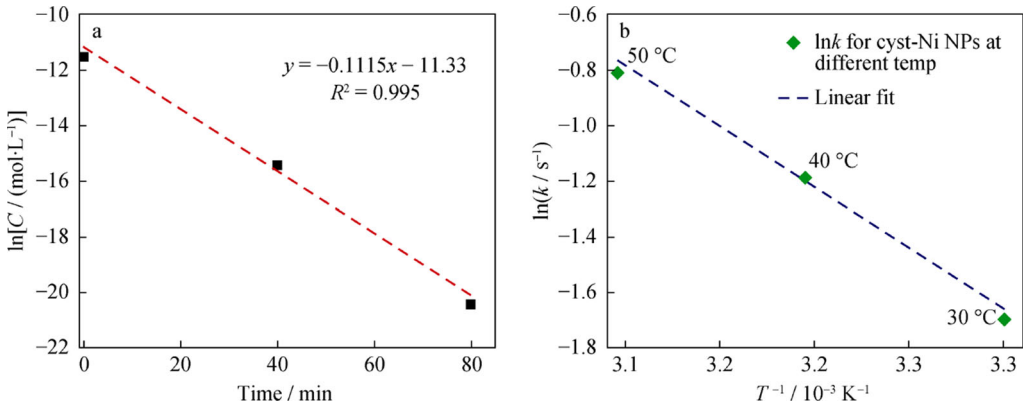

Fig. 10 Linear regression for **a** pseudo-first order kinetics for catalysed reduction and **b** Arrhenius equation with estimation of activation energy of cyst-Ni NPs for reduction of 4-NP

(r^2) of 0.995. The obtained r^2 value clearly shows the catalytic reduction of 4-NPh over cyst–Ni NPs to fit pseudo-first-order kinetics. The catalytic kinetics were further used to determine the activation energy (E_a) of cyst-Ni NPs for the reduction of 4-NPh. Similar catalytic experiments to those described in Sect. 3.6 were carried out at three different temperatures (30, 40 and 50 °C), and the corresponding effective rate constant values of 0.183, 0.306 and 0.446 s^{-1} were used in the following linear Arrhenius equation to estimate apparent activation energy:

$$\ln k = -\frac{E_a}{R} \times \frac{1}{T} + \ln A \quad (4)$$

where E_a is the activation energy, T is the absolute temperature, R is the universal gas constant and A is a constant. Figure 10b shows a linear plot of obtained ln$k$ values against 1/T for reduction at various temperatures.

The apparent activation energy (E_a) was estimated from the slope of the graph to be 36.1 kJ·mol^{-1}. The obtained value resides within the activation energy range of surface catalysed reactions (8–40 kJ·mol^{-1}) [43]. This suggests that the heterogeneous reduction of 4-NPh in our case is a surface phenomenon. The obtained activation energy is much smaller than that reported by several other studies [44–46], which may be attributed to the larger surface area provided by the smaller size of synthesised Ni NPs.

3.8 Reuse of Ni NPs as catalyst

Figure 11 represents the conversion of 4-NPh to 4-APh by freshly prepared and up to four-times reused cyst–Ni NPs used as catalyst. The results show excellent catalytic performance of the reused cyst-Ni NPs and elaborate that the process is highly economised due to high efficiency of the catalyst with negligible poisoning by the solution environment. Furthermore, the recovery and reuse of catalyst provide economic synthesis of 4-APh (with no intermediate

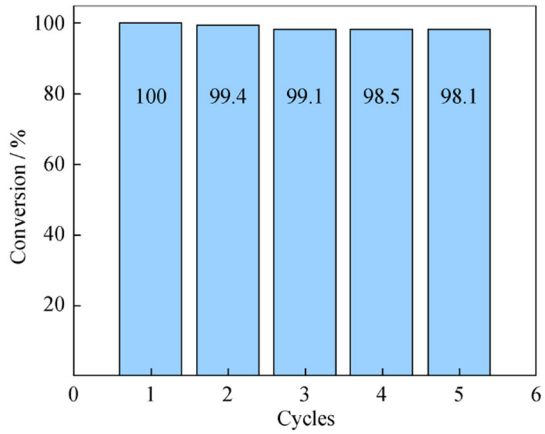

Fig. 11 Histograms showing conversion of 10 μmol·L^{-1} 4-NPh in presence of 10 mmol·L^{-1} $NaBH_4$ solution by fresh and up to four-times regenerated and reused 0.2 mg Ni NPs

formation) for the purpose of its industrial utilisation in the manufacture of analgesics, antipyretics, etc., and hence its subsequent removal from the aquatic environment.

4 Conclusion

In this study, Ni NPs were synthesised using a simple and rapid microwave irradiation method by employing L-cysteine biomolecules as an effective protecting agent and ethylene glycol as solvent. The as-synthesised cyst–Ni NPs are proved to be an excellent heterogeneous catalyst for complete reduction of 4-nitrophenol to 4-aminophenol in reaction time of just 40 s, which makes the process highly efficient and economical. In addition, the study highlights the kinetic and energetic behaviours of Ni NPs during the catalytic reduction of 4-NPh. Furthermore, the recovery and reuse of cyst-Ni NPs with negligible poisoning make the task even more cost effective as well as

environmentally friendly. This work is extendable to the reduction of other phenols as well as other compounds, such as dyes and nitrates.

Acknowledgments This work was financially supported by the King Saud University via their Research Project (No. RGP-VPP-236). The authors acknowledge facilities provided by the National Centre of Excellence in Analytical Chemistry, University of Sindh, Jamshoro, Pakistan Higher Education Commission (HEC), Pakistan, and the Interface Analysis Centre, University of Bristol, Bristol, United Kingdom.

References

[1] Pigozzi G, Mukherji D, Gilles R, Barbier B, Kostorz G. Ni(3)Si(Al)/a-SiO(x) core-shell nanoparticles: characterization, shell formation, and stability. Nanotechnology. 2006;17(16):4195.
[2] Abedini A, Daud A, Abdul Hamid M, Kamil Othman N, Saion E. A review on radiation-induced nucleation and growth of colloidal metallic nanoparticles. Nanoscale Res Lett. 2013;8(1):1.
[3] Shah AT, Din MI, Farooq U, Butt MTZ, Athar M, Chaudhary MA, Ahmad MN, Mirza ML. Fabrication of nickel nanoparticles modified electrode by reverse microemulsion method and its application in electrolytic oxidation of ethanol. Colloid Surf A. 2012;405:19.
[4] Yeom SH, Han ME, Kang BH, Kim KJ, Yuan H, Eum NS, Kang SW. Enhancement of the sensitivity of LSPR-based CRP immunosensors by Au nanoparticle antibody conjugation. Sens Actuat B Chem. 2013;177:376.
[5] Wang XY, Li YJ, Xu C, Kong L, Li L. Synthesis and characterization of $Li_4Ti_5O_{12}$ via a hydrolysis process from $TiCl_4$ aqueous solution. Rare Met. 2014;33(4):459.
[6] Gopal R, Singh MK, Agarwal A, Singh SC, Swarnkar RK. Synthesis of nickel nanomaterial by pulsed laser ablation in liquid medium and its characterization. AIP Conf Proc. 2009;1147(1):199.
[7] Ding XF, Shen JY, Gao XJ, Wang J. Enhanced electrochemical properties of $Sm_{0.2}Ce_{0.8}O_{1.9}$ film for SOFC electrolyte fabricated by pulsed laser deposition. Rare Met. DOI 10.1007/s12598-014-0396-y.
[8] Kalwar NH, Sirajuddin, Sherazi STH, Abro MI, Tagar ZA, Hassan SS, Junejo Y, Khattak MI. Synthesis of L-methionine stabilized nickel nanowires and their application for catalytic oxidative transfer hydrogenation of isopropanol. Appl Catal A-Gen. 2011;400(1–2):215.
[9] Liu QM, Yu RL, Qiu GZ, Fang Z, Chen AL, Zhao ZW. Optimization of separation processing of copper and iron of dump bioleaching solution by Li_xN in Dexing Copper Mine. Trans Nonfer Met Soc. 2008;18(5):1258.
[10] Zhu HT, Zhang CY, Yin YS. Rapid synthesis of copper nanoparticles by sodium hypophosphite reduction in ethylene glycol under microwave irradiation. J Cryst Growth. 2004;270(3–4):722.
[11] Coussy O, Fen-Chong T. Crystallization, pore relaxation and micro-cryosuction in cohesive porous materials. C R Mecanique. 2005;333(6):507.
[12] Athawale AA, Katre PP, Kumar M, Majumdar MB. Synthesis of CTAB–IPA reduced copper nanoparticles. Mater Chem Phys. 2005;91(2–3):507.
[13] Hou Y, Kondoh H, Ohta T, Gao S. Size-controlled synthesis of nickel nanoparticles. Appl Surf Sci. 2005;241(1–2):218.
[14] Roselina NRN, Azizan A, Hyie KM, Jumahat A, Bakar MAA. Effect of pH on formation of nickel nanostructures through chemical reduction method. Proced Eng. 2013;68:43.
[15] Tontini G, Koch A Jr, Schmachtenberg VAV, Binder C, Klein AN, Drago V. Synthesis and magnetic properties of nickel micro urchins. Mater Res Bull. 2015;61:177.
[16] Chinnasamy CN, Jeyadevan B, Shinoda K, Tohji K, Narayanasamy A, Sato K, Hisano S. Synthesis and magnetic properties of face-centered-cubic and hexagonal-close-packed Ni nanoparticles through polyol process. J Appl Phys. 2005;97(10):10J309.
[17] Shinde VM, Madras G. Catalytic performance of highly dispersed Ni/TiO_2 for dry and steam reforming of methane. RSC Adv. 2014;4(10):4817.
[18] Ajeet K, Amit S, Arnab D, Ravi S, Subho M. Controlled synthesis of size-tunable nickel and nickel oxide nanoparticles using water-in-oil microemulsions. Adv Nat Sci Nanosci Nanotechnol. 2013;4(2):025009.
[19] Wu SH, Chen DH. Synthesis and characterization of nickel nanoparticles by hydrazine reduction in ethylene glycol. J Colloid Interface Sci. 2003;259(2):282.
[20] Roy PS, Bhattacharya SK. Size-controlled synthesis, characterization and electrocatalytic behaviors of polymer-protected nickel nanoparticles: a comparison with respect to two polymers. RSC Adv. 2014;4(27):13892.
[21] Kujawa P, Rosiak JM. Pulse radiolysis of 2-[(methacryloyloxy)ethyl]trimethylammonium chloride in aqueous solution. Radiat Phys Chem. 2000;57(3–6):559.
[22] Sun Z, Chen Y, Ke Q, Yang Y, Yuan Y. Photocatalytic degradation of a cationic AZO dye by TiO_2/bentonite nanocomposite. J Photochem Photobiol A. 2002;149(1–3):169.
[23] Du Y, Chen H, Chen R, Xu N. Synthesis of p-aminophenol from p-nitrophenol over nano-sized nickel catalysts. Appl Catal A Gen. 2004;277(1–2):259.
[24] Zhong Z, Subramanian AS, Highfield J, Carpenter K, Gedanken A. From discrete particles to spherical aggregates: a simple approach to the self-assembly of Au colloids. Chem-Eur J. 2005;11(5):1473.
[25] Fischer-Wolfarth J-H, Farmer JA, Flores-Camacho JM, Genest A, Yudanov IV, Rösch N, Campbell CT, Schauermann S, Freund HJ. Particle-size dependent heats of adsorption of CO on supported Pd nanoparticles as measured with a single-crystal microcalorimeter. Phys Rev B. 2010;81(24):241416.
[26] Zhang C, Hwang SY, Peng Z. Size-dependent oxygen reduction property of octahedral Pt–Ni nanoparticle electrocatalysts. J Mater Chem A. 2014;2(46):19778.
[27] Weber A, Seipenbusch M, Kasper G. Size effects in the catalytic activity of unsupported metallic nanoparticles. J Nanopart Res. 2003;5(3–4):293.
[28] Zhong Z, Subramanian AS, Highfield J, Carpenter K, Gedanken A. From discrete particles to spherical aggregates: a simple approach to the self-assembly of Au colloids. Chemistry. 2005;11(5):1473.
[29] Barth A. Infrared spectroscopy of proteins. Biochim Biophys Acta. 2007;1767(9):1073.
[30] Sirajuddin, Nafady A, Afridi HI, Sara S, Shah A, Niaz A. Direct synthesis and stabilization of Bi-sized cysteine-derived gold nanoparticles: reduction catalyst for methylene blue. J Iran Chem Soc. 2011;8(1):S34.
[31] Yoon M, Kim Y, Kim YM, Volkov V, Song HJ, Park YJ, Park IW. Superparamagnetic properties of nickel nanoparticles in an ion-exchange polymer film. Mater Chem Phys. 2005;91(1):104.
[32] Ma Z, Han H. One-step synthesis of cystine-coated gold nanoparticles in aqueous solution. Colloid Surf A. 2008;317(1–3):229.
[33] Chou KS, Lai YS. Effect of polyvinyl pyrrolidone molecular weights on the formation of nanosized silver colloids. Mater Chem Phys. 2004;83(1):82.
[34] Watzky MA, Finke RG. Transition metal nanocluster formation kinetic and mechanistic studies. A new mechanism when

hydrogen is the reductant: slow, continuous nucleation and fast autocatalytic surface growth. J Am Chem Soc. 1997;119(43):10382.
[35] Hu J, Odom T, Lieber C. Chemistry and physics in one dimension: synthesis and properties of nanowires and nanotubes. Acc Chem Res. 1999;32(5):435.
[36] Soomro RA, Nafady A, Sirajuddin, Memon N, Sherazi TH, Kalwar NH. L-cysteine protected copper nanoparticles as colorimetric sensor for mercuric ions. Talanta. 2014;130:415.
[37] Seol SK, Kim D, Jung S, Chang WS. One-step synthesis of PEG-coated gold nanoparticles by rapid microwave heating. J Nanomater. 2013;2013:6.
[38] Sahoo PK, Kalyan Kamal SS, Kumar TJ, Sreedhar B, Singh AK, Srivastava SK. Synthesis of silver nanoparticles using facile wet chemical route. Def Sci J. 2009;59(4):447.
[39] Chaudhari A, Yan C-CS, Lee SL. Autopoisoning reactions over rough surface: a multifractal scaling analysis. Int J Chem Kinet. 2005;37(3):175.
[40] Lee S-L, Lee C-K. Heterogeneous reactions over fractal surfaces: a multifractal scaling analysis. Int J Quantum Chem. 1997;64(3):337.
[41] Chandra S, Kumar A, Tomar PK. Synthesis of Ni nanoparticles and their characterizations. J Saudi Chem Soc. 2014;18(5):437.
[42] Sharma NC, Sahi SV, Nath S, Parsons JG, Gardea-Torresdey JL, Pal T. Synthesis of plant-mediated gold nanoparticles and catalytic role of biomatrix-embedded nanomaterials. Environ Sci Technol. 2007;41(14):5137.
[43] Zhu Z, Guo X, Wu S, Zhang R, Wang J, Li L. Preparation of nickel nanoparticles in spherical polyelectrolyte brush nanoreactor and their catalytic activity. Ind Eng Chem Res. 2011;50(24):13848.
[44] Jiang Z, Xie J, Jiang D, Jing J, Qin H. Facile route fabrication of nano-Ni core mesoporous-silica shell particles with high catalytic activity towards 4-nitrophenol reduction. Cryst Eng Commun. 2012;14(14):4601.
[45] Ozay H. Comparison study of low cost fly ash supported Cu, Co and Ni metal catalyst systems for the reduction of 4-nitrophenol. Sci Adv Mater. 2013;5(6):575.
[46] Wu XQ, Wu XW, Shen JS, Zhang HW. In situ formed metal nanoparticle systems for catalytic reduction of nitroaromatic compounds. RSC Adv. 2014;4(90):49287.